



Universiteit
Leiden
The Netherlands

Evidence of cerebral hypoperfusion consecutive to ultrasound-mediated blood-brain barrier opening in rats

Labriji, W.; Clauzel, J.; Mestas, J.L.; Lafond, M.; Lafon, C.; Salabert, A.S.; ... ; Desmoulin, F.

Citation

Labriji, W., Clauzel, J., Mestas, J. L., Lafond, M., Lafon, C., Salabert, A. S., ... Desmoulin, F. (2023). Evidence of cerebral hypoperfusion consecutive to ultrasound-mediated blood-brain barrier opening in rats. *Magnetic Resonance In Medicine*, 89(6), 2281-2294.
doi:10.1002/mrm.29596

Version: Publisher's Version
License: [Creative Commons CC BY 4.0 license](https://creativecommons.org/licenses/by/4.0/)
Downloaded from: <https://hdl.handle.net/1887/3754512>

Note: To cite this publication please use the final published version (if applicable).

RESEARCH ARTICLE

Magnetic Resonance in Medicine

Evidence of cerebral hypoperfusion consecutive to ultrasound-mediated blood-brain barrier opening in rats

Wafae Labriji¹ | Julien Clauzel¹ | Jean-Louis Mestas² | Maxime Lafond² | Cyril Lafon² | Anne-Sophie Salabert^{1,3} | Lydiane Hirschler⁴ | Jan M. Warnking⁵ | Emmanuel L. Barbier⁵ | Isabelle Loubinoux¹ | Franck Desmoulin^{1,6}

¹ToNIC, Toulouse NeuroImaging Center, Université de Toulouse, INSERM, UPS, Toulouse, France

²LabTAU, INSERM, Centre Léon Bérard, Université Lyon 1, Univ Lyon, F-69003, Lyon, France

³Centre Hospitalo-Universitaire de Toulouse, Toulouse, France

⁴Department of Radiology, C. J. Gorter Center for High Field MRI, Leiden University Medical Center, Leiden, The Netherlands

⁵U1216, Grenoble Institut Neurosciences, Univ. Grenoble Alpes, Inserm, Grenoble, France

⁶CREFRE-Anexplo, Université de Toulouse, INSERM, UPS, ENVT, Toulouse, France

Correspondence

Franck Desmoulin, ToNIC, Toulouse NeuroImaging Center, Université de Toulouse, INSERM, UPS, Toulouse, France.

Email: franck.desmoulin@inserm.fr

Funding information

Agence Nationale de la Recherche, Grant/Award Number:

ANR-19-ASTR-0027; Fondation des Gueules Cassées, Grant/Award Numbers: 70-2019, 22-2022

Purpose: This work aims to explore the effect of Blood Brain Barrier (BBB) opening using ultrasound combined with microbubbles injection on cerebral blood flow in rats.

Methods: Two groups of $n = 5$ rats were included in this study. The first group was used to investigate the impact of BBB opening on the Arterial Spin Labeling (ASL) signal, in particular on the arterial transit time (ATT). The second group was used to analyze the spatiotemporal evolution of the change in cerebral blood flow (CBF) over time following BBB opening and validate these results using DSC-MRI.

Results: Using pCASL, a decrease in CBF of up to $29.6 \pm 15.1\%$ was observed in the target hemisphere, associated with an increase in arterial transit time. The latter was estimated to be $533 \pm 121\text{ms}$ in the BBB opening impacted regions against $409 \pm 93\text{ms}$ in the contralateral hemisphere. The spatio-temporal analysis of CBF maps indicated a nonlocal hypoperfusion. DSC-MRI measurements were consistent with the obtained results.

Conclusion: This study provided strong evidence that BBB opening using microbubble intravenous injection induces a transient hypoperfusion. A spatiotemporal analysis of the hypoperfusion changes allows to establish some points of similarity with the cortical spreading depression phenomenon.

KEYWORDS

blood brain barrier opening, brain perfusion, DSC, MRI, pCASL, rodent, ultrasound

Abbreviations: BBB, Blood Brain Barrier; CBF, cerebral blood flow; ASL, Arterial Spin Labeling; DSC, Dynamic Susceptibility Contrast; CSD, Cortical Spreading Depression.

Wafae Labriji and Julien Clauzel contributed equally to this work.

This is an open access article under the terms of the [Creative Commons Attribution-NonCommercial License](https://creativecommons.org/licenses/by-nc/4.0/), which permits use, distribution and reproduction in any medium, provided the original work is properly cited and is not used for commercial purposes.

© 2023 The Authors. *Magnetic Resonance in Medicine* published by Wiley Periodicals LLC on behalf of International Society for Magnetic Resonance in Medicine.

1 | INTRODUCTION

Neurodegenerative diseases and cerebral tumors affect millions of people worldwide. Clinical and preclinical research are actively working to improve our understanding of these neurological pathologies and provide effective treatments to reduce the progression of the associated symptoms. However, the essential role that the Blood-Brain Barrier (BBB) plays in regulating inputs to the brain is becoming a critical constraint in the development of pharmacological treatments. Indeed, only drugs with a molecular weight smaller than 400 Da can naturally cross the BBB.¹ Major efforts have been deployed to overcome this problem.²

Several studies have explored the potential of ultrasound to disrupt the BBB in order to overcome this limitation.³ The method selected for its low tissue damage, reversibility and transient nature^{4,5} is the use of low intensity pulsed ultrasound combined with microbubble intravenous injection (MB+US). The change in acoustic pressure causes microbubble to oscillate, expand, and contract, producing mechanical forces on the vessel walls that temporarily increase the BBB permeability. Despite the fact that this phenomenon is still poorly understood, several hypotheses exist. Thus, to avoid irreversible tissue damage, it is recommended to adopt a stable cavitation regime, that is, that the resulting microbubble size oscillation is stable, and stay away from the inertial cavitation regime as it can break down membranes of nearby cells and is more likely to induce edema or hemorrhage.^{6,7} Stable cavitation generates mechanical stress on BBB endothelial cells, depending on the ultrasound amplitude and frequency, and microbubble size relative to that of the blood vessels. Ultrasound combined with microbubble injection enhances the passage of molecules across the BBB by various means,⁸ but predominantly through the paracellular pathway due to the enlargement of tight junctions under the effect of the induced mechanical stress.⁹

Complex regulatory mechanisms are involved to maintain the equilibrium between perfusion supply and brain tissue consumption; such as myogenic tone, neurogenic response, metabolic mechanism, and endothelial mechanism.¹⁰ In order to progressively translate into clinical trials,¹¹ many preclinical studies have been conducted to investigate the safety profile of the BBB opening procedure in healthy mammals. This showed a reduction in neurovascular response following the BBB disruption.¹² As cerebral perfusion enables the oxygen supply necessary for the oxidative metabolism process of neurons, it is highly important to investigate any secondary effect of US-induced BBB opening on cerebral perfusion. Recently, a functional-MRI study of the neurovascular response

after MB+US-induced BBB opening demonstrated an attenuated hemodynamic response to both external stimulation and hypercapnia challenge.¹³ Apart from a recent study,¹⁴ the effects of BBB opening on cerebral blood flow have been under-studied, and several questions related to this topic remain unanswered.¹⁵

The aim of this work is to investigate the effect of BBB opening by MB+US on cerebral perfusion measured by MRI in rats. Several techniques are used to quantify CBF using MRI: exogenous labeling methods, based on dynamic tracking of contrast agent transit, and endogenous methods based on arterial spin labeling (ASL) of blood water.^{16,17} A first experiment was conducted to explore the impact of this procedure on the ASL signal and the associated estimation of cerebral blood flow and arterial transit time (ATT), using the pCASL (pseudo-Continuous Arterial Spin Labeling) MRI sequence.¹⁸ This experiment enabled the analysis of CBF maps from 40–60 min after the opening of the BBB and the assessment of ATT in the impacted area. The outcomes motivated a second experiment, focused on studying, at an early stage of BBB opening, the spatiotemporal evolution of CBF change using pCASL. A DSC-MRI¹⁹ (dynamic susceptibility contrast MRI) acquisition was used to validate and complete the obtained results.

2 | METHODS

2.1 | Animal preparation

Animals were treated according to the Council of the European Communities guidelines (EU Directive 2010/63). This protocol was approved by the “Direction Départementale de la Protection des Populations de la Haute – Garonne” and the “Comité d'éthique pour l'expérimentation animale Midi-Pyrénées” (protocol number 16780).

Ten healthy Wistar female rats (Janvier Labs) were used with five animals (13–18 weeks old, weight: 300 ± 20 g) included in the first experimental group (Experiment 1) and five animals (34–38 weeks old, weight: 400 ± 30 g) included in the second experimental group (Experiment 2). Animals were first anesthetized using an induction chamber with 3% of Isoflurane/O₂. A catheter was placed on the rat lateral tail vein while anesthetized with 2% of Isoflurane/O₂ over a heating plate. The catheter has been used for both microbubble injection and contrast agent injection. For the imaging experiments, animals were placed in a dedicated rat head Imaging Cell (Equipement Vétérinaire Minerve SA) which allows to preserve the animal health status (specific-pathogen-free)

where Isoflurane/O₂ level was delivered from a nose cone and maintained at 2%. The imaging cell enables temperature regulation through heated air channels such that the animal's body temperature was kept constant to $37 \pm 0.5^\circ\text{C}$. Respiratory rate was maintained around 60 ± 10 breaths per min. All animal handling was carried out in a biological safety cabinet.

The animals received a dose of 0.5 mmol/kg of Gadolinium (Dotarem[®]) followed by a 300 μl flush of saline.

2.2 | BBB opening procedure: MB+US

To ensure good coupling between the transducer and the skull, the animal's head was shaved with an electrical razor and depilatory cream. An ultrasonic gel couplant was then applied to the shaved surface of the animal's head. Prior to sonication, animals received an injection of 200 μl of microbubbles (SONOVUE, 8 $\mu\text{l}/\text{ml}$ Bracco[®]) followed by a 300 μl flush of saline. Sonovue microbubbles consist of an ultrasound contrast agent composed of sulfur hexafluoride trapped in phospholipid microspheres with an average diameter of about $2.5 \mu\text{m}^{20}$ at atmospheric pressure.

Pulsed ultrasound were induced in the right hemisphere of rat brains with a 10 mm flat transducer operating at a center frequency of 1.13 MHz. The sonication parameters were adjusted in agreement with previous studies.^{5,21} The 25 ms duration 1.13 MHz sine pulses has been created using a function generator (HP33120A, Hewlett-Packard) at a pulse repetition frequency of 1 Hz. The signal was then amplified by a LA200H power amplifier (Kalmus Engineering) and transmitted to the 50 Ω transducer (in-house impedance matching network). The overall sonication time was set to 2 min. These conditions allow BBB opening with limited damage to healthy tissue.^{5,21} A preliminary experiment was performed to identify 0.5 MPa as the minimum acoustic pressure required to induce effective BBB opening (see Appendix S1).

Thus, experiments were conducted at 0.5 MPa (as calibrated in water) which corresponds to 0.38 MPa and 0.30 MPa accounting for the 25% and 40% attenuation loss due to transmission through the skull in the first and second animal group, respectively.²²

2.3 | Magnetic resonance imaging

Animals were imaged on a 7T preclinical MRI scanner (Biospec 70/16) equipped with a volume transmit coil and a 2×2 elements surface receive coil. Anatomical T₂-weighted (T_{2w}) images were acquired using a spin-echo sequence (TR/TE = 2500/33 ms; in-plane resolution,

$0.137 \times 0.137 \text{ mm}^2$; slice thickness, 1 mm; RARE-factor, 8; acquisition time $T_{\text{acq}} = 2 \text{ min } 40 \text{ s}$). For CBF quantification, and to confirm BBB opening, T₁ maps of the brain tissue T₁(T_{1,t}) were acquired with a nonselective inversion recovery spin-echo Echo Planar Imaging (EPI) sequence (pulse repetition time [TR]/echo time [TE] = 10 000/15 ms; in-plane resolution, $0.326 \times 0.326 \text{ mm}^2$; slice thickness, 1 mm; 17 inversion times (TI) between 20 and 9000 ms; number of averages NA = 2; $T_{\text{acq}} = 5 \text{ min } 40 \text{ s}$).

The pCASL sequence applied in the two protocols described hereafter uses an unbalanced pCASL scheme (with null mean gradient during the Control acquisitions) preceded by two interpulse phase correction prescans designed to reduce the tagging efficiency loss in pCASL and improve CBF estimation accuracy.²³

Blood water spins were inverted using a localized labeling plane placed at the level of the rat neck (at 10 mm from the magnet isocenter and 20 mm from the anterior commissure). The labeling pulse train consisted of 400 μs Hanning-window-shaped RF pulses repeated every 800 μs and scaled to an average B1 amplitude of 3.5 μT during the RF pulse train. $G_{\text{max}}/G_{\text{mean}}$ were set to 45/5 mT/m.

Following the phase optimization scans for each Label and Control set, the resulting inversion efficiency (IE) was measured 5 mm downstream the label plane with a flow compensated gradient-echo sequence.

All EPI acquisitions were performed after a global second order shimming over the brain volume (Map Shim Bruker protocol) to minimize the geometric distortions related to the EPI readout without strongly affecting the field homogeneity at the level of the labeling slice.

2.3.1 | Experiment 1

After the animal preparation and the MB+US BBB opening (BBBO) localized on the right hemisphere ($n=5$), images were acquired with the experimental time line given in Figure 1, as following:

- Anatomical T_{2w} image,
- T₁ map (before contrast agent injection) (T_{1,pre-Gado}),
- pCASL phase optimization step and Inversion Efficiency measurements,
- Five pCASL scans with different post-labeling-delays: PLDs = [300 10 1100 200 700] ms and a labeling time of: LT = 2 s (TR/TE = 3100/15 ms; in-plane resolution, $0.326 \times 0.326 \text{ mm}^2$; slice thickness, 2 mm; number of repetitions: NR = 35 interleaved Label/Control scans; $T_{\text{acq}} = 3 \text{ min}$),
- T₁ map (after contrast agent injection) (T_{1,post-Gado}).

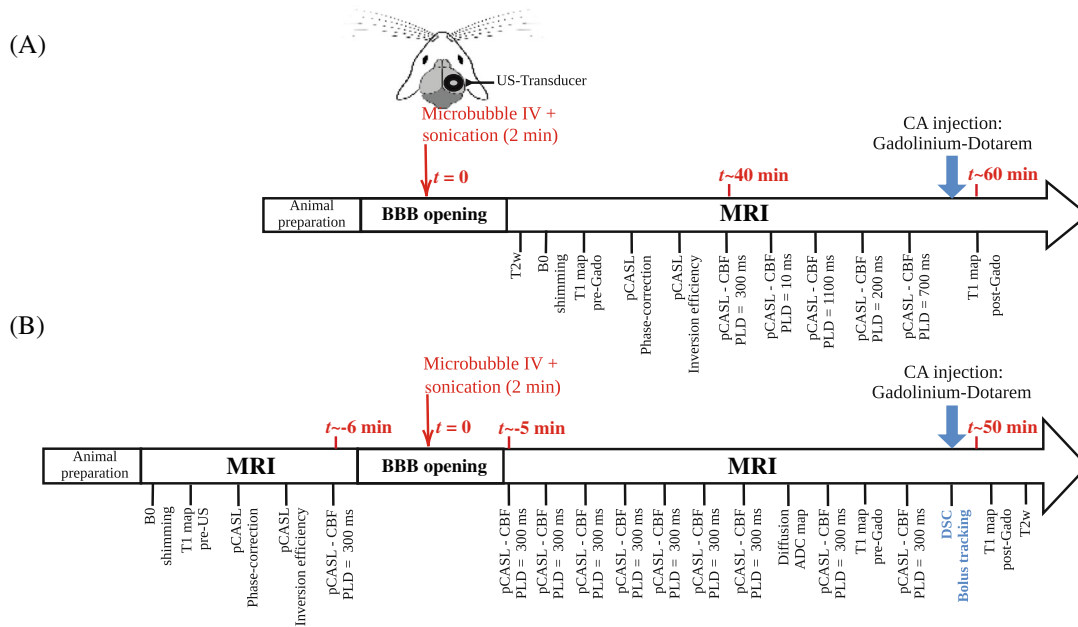


FIGURE 1 Experimental time line that describes the two experiments conducted in this study. For both, the opening of the Blood Brain Barrier was performed outside the magnet under a bio-safety cabinet and Gado-Dota intravenous injection have been conducted 50 min after. The time $t = 0$ corresponds to the ending of the sonication. (A) Experiment 1; (B) Experiment 2

2.3.2 | Experiment 2

To describe the spatiotemporal evolution; a second experimental protocol, given in Figure 1, was designed including CBF estimation before and several minutes after MB+US BBB opening ($n = 5$). Acquisitions were successively:

Before BBB opening:

- T_1 map (before sonication) ($T_{1,pre-US}$),
- pCASL phase correction step and IE measurements,
- One pCASL scan for reference CBF quantification with a single post labeling delay (PLD) = 300 ms and a labeling time of $LT = 2$ s (TR/TE = 2600/15 ms; in-plane resolution, 0.326×0.326 mm²; slice thickness, 1 mm; number of repetitions: NR = 35 interleaved Label/Control scans; $T_{acq} = 3$ min).

Special caution was taken to keep the animal cell in the same location in the magnet in order to ensure a consistent high IE of the pCASL scans since the measured phase corrections are strongly correlated with the resonance frequency in the carotids at the labeling plane.²³

After BBB opening:

- A set of pCASL acquisitions (nine scans) acquired directly after putting back the animal in the magnet (between 5 and 8 min following BBB procedure),
- Diffusion map with EPI readout for apparent diffusion constant (ADC) quantification were acquired at b-values of 0 and 800 s/mm² and three diffusion

directions (TR/TE = 2500/20 ms; in-plane resolution, 0.326×0.326 mm²; slice thickness, 1 mm; $T_{acq} = 3$ min 20 s),

- T_1 map (after sonication and before Gadolinium injection) ($T_{1,pre-Gado}$),
- Dynamic susceptibility contrast (DSC) scan with an IV CA injection 30 s after the beginning of the acquisition (TR/TE = 500/10 ms; in-plane resolution, 0.390×0.390 mm²; slice thickness, 1 mm; for 300 scans during 2 min 30 s),
- T_1 map (after Gadolinium injection) ($T_{1,post-Gado}$)
- Anatomical T_2W image.

2.4 | Data processing

The MRI data were reconstructed and analyzed using MP3 software²⁴ developed in Matlab (The MathWorks Inc). Before any processing, all EPI acquisitions were realigned to correct for any possible movement of the animal during the experiment using ANTs. For each pCASL scan, the repetitions were realigned to the first volume and all EPI acquisitions have been realigned to a pCASL averaged volume acquired in the middle of the experiment.

2.4.1 | Selection of regions of interest

The BBB-disrupted (or BBBO) region was identified using the difference between T_1 maps obtained before and after

the Gado-Dota injection. BBBO regions are regions such that

$$\Delta T_1 = (T_{1,\text{pre-Gado}} - T_{1,\text{post-Gado}}) > 50 \text{ ms.} \quad (1)$$

The 50 ms threshold value was chosen based on the obtained results of ΔT_1 values in the unexposed hemisphere. Indeed, following injection of a gadolinium-based contrast agent, the T_1 relaxation time of the tissues decreases moderately, in part due to residual intravascular gadolinium, as reported in previous studies.²⁵ CBF map analysis was made for the whole brain and in cortical, hippocampal, thalamic, and striatal regions. Then, results are displayed for the whole brain and the cortex. This choice was motivated by the disparity of effects observed in the rest of the structures between the different subjects of the study.

To compare and normalize the BBBO results, the analyses were also performed on the contralateral regions obtained from the symmetric of the US exposed regions with respect to the brain midline. In addition to this, complementary regions to the BBBO regions were considered. The complementary regions describe the voxels of the exposed hemisphere that do not fulfill the above mentioned condition: $\Delta T_1 > 50 \text{ ms}$.

2.4.2 | T_1 mapping

T_1 maps were obtained by fitting signal evolution as a function of the TI pixel by pixel to the following equation using the Levenberg–Marquardt algorithm:

$$M_z(\text{TI}) = |M_0 \cdot \left(1 - 2 \cdot \kappa e^{-\frac{\text{TI}}{T_{1,t}}}\right)|, \quad (2)$$

where $M_z(\text{TI})$ is the MR signal collected at each TI, M_0 is the magnetization at thermal equilibrium, $T_{1,t}$ is the longitudinal relaxation time constant of the tissue, and κ is the IE.

2.4.3 | Apparent diffusion constant

ADC has been automatically computed by the online processing tool included in the ParaVision 6.1 software package of the MRI scanner.

2.4.4 | Arterial transit time

ATT is defined as the duration for the tagged blood to flow from the labeling plane to the vascular or the tissue compartments. It has been estimated in parallel with CBF assessment of Experiment 1 using

the Levenberg–Marquardt algorithm to approximate ASL signal $\Delta M/M_c$ evolution as function of PLD as given by the Buxton model²⁶ where ΔM is the signal difference between control and label acquisitions averaged over repetitions. This estimation is based on one additional hypothesis: CBF and ATT change during multi-PLD pCASL acquisitions is considered to be negligible.

2.4.5 | pCASL - CBF maps

pCASL - CBF maps of Experiment 2 were computed using the general kinetic model for quantitative perfusion imaging with ASL,²⁶ while considering a single compartment model based on the assumption that the rate of exchange between the vascular environment and the brain tissue is extremely fast. Assuming that the postlabeling delay is higher than the ATT, one has:

$$\text{CBF} = \frac{6000 \cdot \lambda \cdot \Delta M \cdot e^{-\frac{\Delta t}{T_{1,b}}} \cdot e^{-\frac{\text{PLD}-\Delta t}{T_{1,t}}}}{2 \cdot \text{IE} \cdot T_{1,t} \cdot M_{0,t} \cdot \left(1 - e^{-\frac{\tau}{T_{1,t}}}\right)} \quad (3)$$

where $T_{1,t}$ is the apparent T_1 of tissue obtained from the T_1 map; $T_{1,b}$ is the longitudinal relaxation time of blood (2230 ms at 7T);²⁷ $M_{0,t}$ is the tissue magnetization at thermal equilibrium, τ is the labeling time, Δt is the ATT, λ the brain-blood partition coefficient of water (0.9 ml/g)²⁸ and IE. $M_{0,t}$ was estimated using the control image of the ASL experiment multiplied by $[1 - e^{-\frac{\text{TR}}{T_{1,t}}}]^{-1}$ to correct for incomplete T_1 relaxation during the TR.

For pCASL-CBF quantification of Experiment 2, the ATT (Δt) has been fixed to 300 ms.^{29,30}

2.4.6 | DSC - perfusion measurements

DSC - Perfusion measurements have been computed using the DSC-MRI toolbox.³¹ The arterial input function was identified semi-automatically, and contrast extravasation correction was performed using an algorithm based on T_1 enhancement suppression that decreases the estimated relative quantification of cerebral blood volume (rCBV) artifactually.³² DSC analyses provided relative quantification of cerebral blood flow (rCBF), rCBV, and mean transit time.

2.4.7 | Visualization of the spatiotemporal evolution of CBF in the Cortex

This visualization is to study the propagation of CBF alteration in rat cortex, that can be approximated by a circular section on a two-dimensional slice, we extracted the

spatial evolution over time of the ASL signal from the middle dorsal side to the lateral side of the cortex. To do so, we converted our matrix, initially in cartesian coordinates, into polar coordinates (r, θ). The center of the new system has been defined by considering a circle that best crosses the different voxels of the cortical area. This allows to consider a constant average radius throughout the cortex. An angular step of 0.5° has been chosen in order to properly sample the evolution of the signal. Then, the voxels contributions have been averaged given the considered angular step. This process has been performed for each of the 35 repetitions of the 10 pCASL scans of Experiment 2 to obtain ASL signal evolution maps along the cortex over pCASL scans. The obtained maps were finally highly smoothed with a two-dimensional Gaussian filter. The propagation speed was calculated from the level curves plotted on the obtained maps, considering $v = (R \cdot \Delta\theta) / \Delta t$ with R the average radius, $\Delta\theta$ the angle range and Δt the time range obtained as $\Delta t = n \cdot 2 \cdot TR$, with TR pCASL repetition time (for each *Label/Control*) and n the number of scans.

2.5 | Statistical analysis

All data are expressed as mean \pm SD. Paired *t*-test or Wilcoxon test (when normality test failed) have been used to evaluate the differences between BBBO regions and

contralateral regions in the case of DSC perfusion maps and to evaluate the significant decrease and recovery of CBF obtained from pCASL scans. Normal distribution hypothesis have been tested using the Anderson-Darling test. A *p*-value < 0.05 was considered significant. Pearson correlation coefficient has been used to evaluate the linear correlation between pCASL-CBF and DSC-rCBF measurements.

3 | RESULTS

3.1 | Experiment 1

Figure 2 displays typical T_1 maps acquired before and after Gadolinium injection. Contrast agent injection was performed 60 min following BBB opening. ΔT_1 , obtained from the subtraction of the tissue T_1 before and after contrast agent injection has been thresholded at $\Delta T_1 > 50$ ms based on the obtained values over the control hemisphere found to be $\Delta T_{1, \text{no-BBBO}} = 38.9 \pm 13.8$ ms ($T_{1, \text{pre-Gado}} = 1610.9 \pm 37.4$ ms and $T_{1, \text{post-Gado}} = 1572.0 \pm 46.7$ ms). Meanwhile, $\Delta T_{1, \text{BBBO}} = 233.1 \pm 183.6$ ms was found on the US-exposed hemisphere ($T_{1, \text{pre-Gado}} = 1660.8 \pm 36.1$ ms and $T_{1, \text{post-Gado}} = 1427.8 \pm 150.9$ ms). Significant difference is found between $\Delta T_{1, \text{BBBO}}$ and $\Delta T_{1, \text{no-BBBO}}$ and confirms the effective opening of the BBB in the

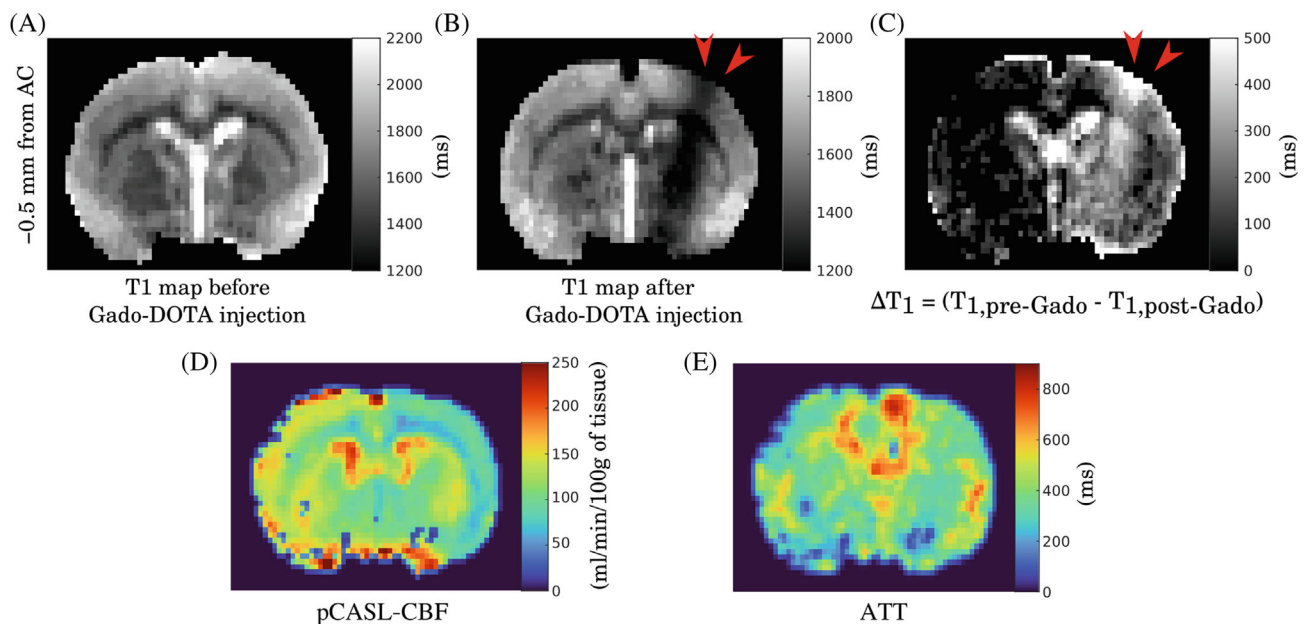


FIGURE 2 Coronal T_1 maps (A) before and (B) after Gadolinium injection for one typical subject. T_1 decrease is indicative of Blood Brain Barrier (BBB) permeation to Gado-Dota and allows to locate the BBB opening area. (C) was obtained from the subtraction of the tissue T_1 before and after Gadolinium injection. To highlight the effective opening of the BBB, values less than 50 ms were set to zero. (D) Corresponding cerebral blood flow and (E) arterial transit time maps with a nonlocal blood flow decline associated with delayed arterial transit time in the US-exposed hemisphere (AC, anterior commissure). The red arrows shown in (B) and (C) indicate the positioning of the transducer over the right hemisphere of the animal.

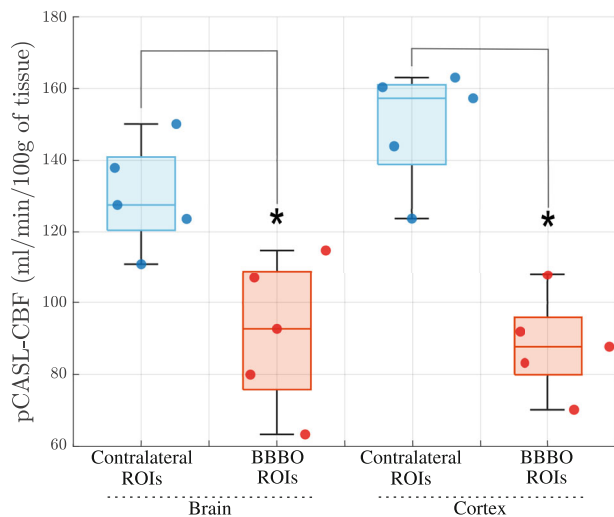


FIGURE 3 Cerebral blood flow assessment computed over blood brain barrier opening and contralateral regions in the whole hemisphere ($p = 0.01$; paired t -test) and cortex ($p = 0.008$; paired t -test), respectively for the Experiment 1 ($n = 5$)

US-exposed hemisphere ($p = 0.008$; Wilcoxon rank sum test), with a mean volume of $203.3 \pm 70.7 \text{ mm}^3$.

The corresponding obtained CBF map, on Figure 2, illustrate a visible decrease in cerebral perfusion over the sonicated region combined with a slight increase in the ATT. Computed CBF values for BBBO regions (whole brain) and BBBO cortical regions, for the five rats, are displayed in Figure 3. Absolute CBF quantification taking into account the ATT through multi-PLD acquisitions indicated a $29.6 \pm 15.1\%$ decrease between BBBO regions ($\text{CBF}_{\text{BBBO}} = 91.5 \pm 20.7 \text{ ml/min/100g of tissue}$) compared to the contralateral region ($\text{CBF}_{\text{no-BBBO}} = 130.0 \pm 14.8 \text{ ml/min/100g of tissue}$) ($p = 0.01$; paired t -test). The same measurements performed only on the cortical areas allows to obtain a similar result (a decrease of $41.1 \pm 16.2\%$ with $\text{CBF}_{\text{BBBO}} = 88.1 \pm 13.7 \text{ ml/min/100g of tissue}$ against $\text{CBF}_{\text{no-BBBO}} = 149.6 \pm 16.2 \text{ ml/min/100g of tissue}$) ($p = 0.008$; paired t -test).

pCASL-multi PLD scans allowed to reconstruct the ASL signal evolution according to the postlabeling time as shown in Figure 4. The ASL signal evolution as a function of PLD reveals a delayed transit time in the BBBO region compared to the contralateral region. Indeed, the mean measured ATT over the BBBO regions ($\text{ATT}_{\text{BBBO}} = 533 \pm 121 \text{ ms}$) is higher than the estimated ATT in the contralateral hemisphere ($\text{ATT}_{\text{no-BBBO}} = 409 \pm 93 \text{ ms}$) ($p = 0.04$; Wilcoxon signed-rank test).

3.1.1 | Experiment 2

Calculated T_1 maps for the second experiment are similar to those described in Figure 2. The results show a decrease

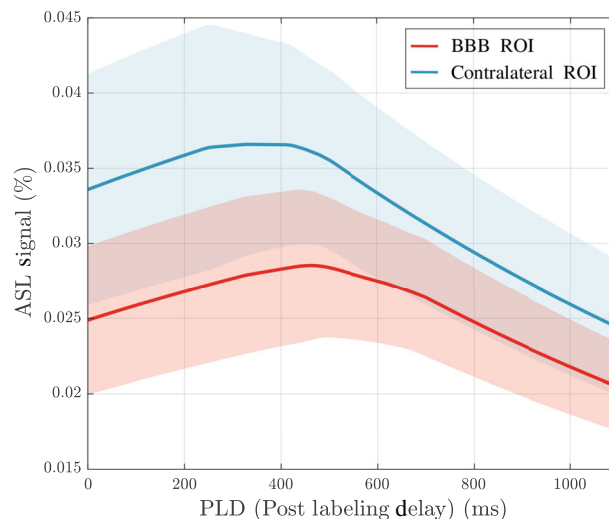


FIGURE 4 Arterial spin labeling signal evolution according to the post labeling delay for the blood brain barrier opening region and the contralateral region following a single compartment model fit.²⁶ The solid line is the mean over $n = 5$ rats and the shaded regions depict the SD error.

of tissue T_1 after Gado-Dota injection at the level of the US-exposed hemisphere ($T_{1,\text{pre-Gado}} = 1702.8 \pm 21.4 \text{ ms}$ and $T_{1,\text{post-Gado}} = 1480.0 \pm 221.2 \text{ ms}$) in comparison with the contralateral hemisphere ($T_{1,\text{pre-Gado}} = 1693.0 \pm 67.9 \text{ ms}$ and $T_{1,\text{post-Gado}} = 1625.7 \pm 58.8 \text{ ms}$). Indeed, significant difference has been found between the obtained ΔT_1 at the level of the US-exposed hemisphere ($\Delta T_{1,\text{BBBO}} = 226.5 \pm 225.4 \text{ ms}$) in comparison with the contralateral hemisphere ($\Delta T_{1,\text{no-BBBO}} = 63.6 \pm 23.4 \text{ ms}$) ($p = 0.03$; Wilcoxon rank sum test).

Typical CBF maps obtained over the experiment duration are presented in Figure 5. One can observe the reduction in CBF at the level of the exposed hemisphere, followed by a gradual recovery. However, different structures of the US-exposed hemisphere were not affected in the same way by CBF alterations.

The extracted CBF profiles are presented on Figure 6 for BBBO ROIs and cortical BBBO ROIs. Following temporal interpolation, the obtained CBF estimation has been double normalized to contralateral CBF and reference CBF (acquired before BBBO) in order to reduce intersubject variability. CBF estimation at $t = 0$ is assumed to be equal to the reference value of CBF.

For each profile, CBF evolution is described for the BBBO region and the complementary, that is, with no evidence of BBB opening (revealed by no Gado-Dota extravasation). Displayed profiles have a similar pattern showing a sharp decrease followed by a partial recovery after 50 min. Thus, on the whole hemisphere, CBF decreased at 14 minutes by $22.3\% \pm 5.8\%$ ($p = 0.03$; paired t -test) for BBBO regions and $14.7\% \pm 8.9\%$ for the

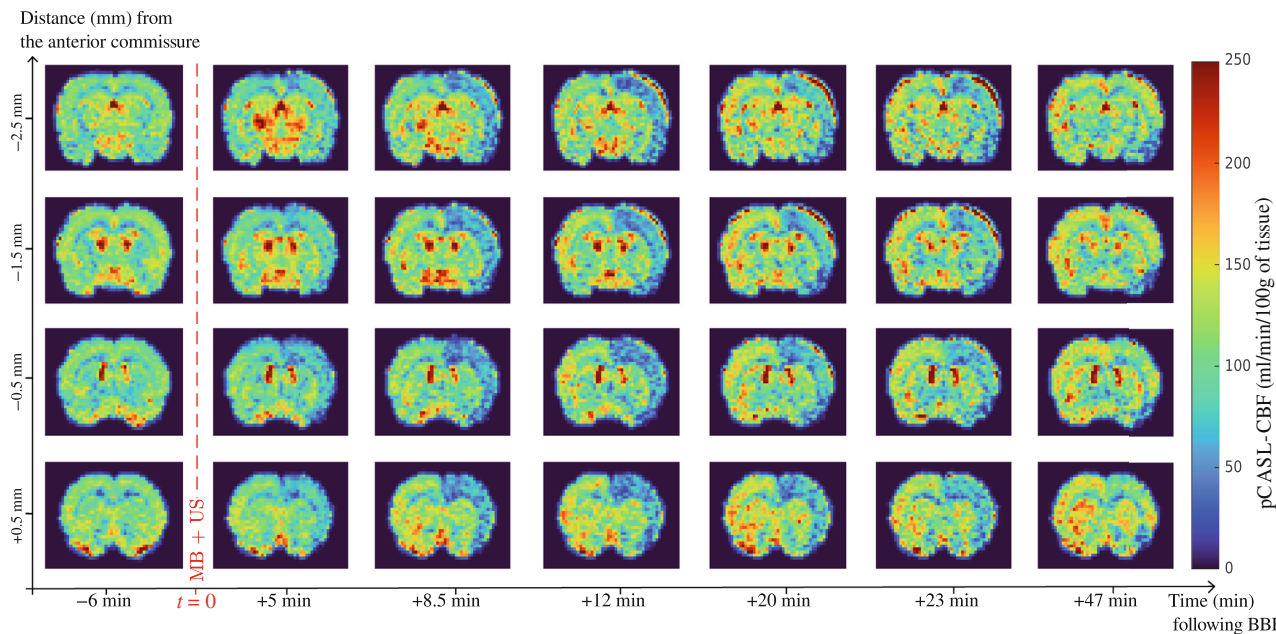


FIGURE 5 Coronal slices cerebral blood flow (CBF) maps depicts blood flow evolution during the Experiment 2 for one rat, measured before and several times following blood brain barrier opening procedure. Altered CBF is clearly visible: a first phase of CBF decrease is followed by a progressive recovery with an estimated recovery in the 50 min following sonication.

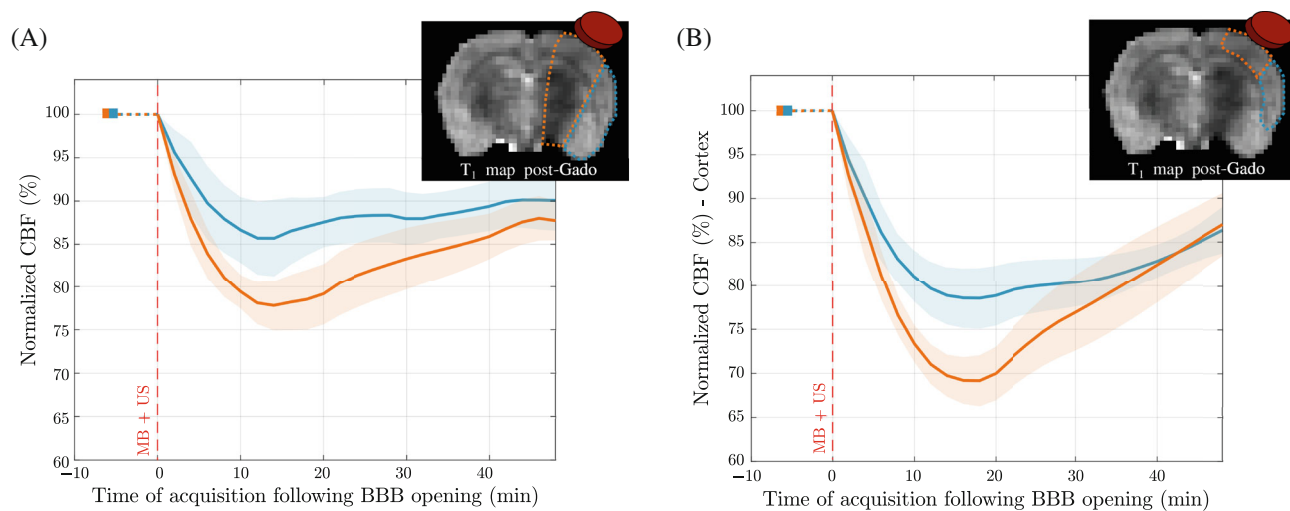


FIGURE 6 Temporal normalized cerebral blood flow (CBF) profiles for the blood brain barrier (BBB) opening (BBBO) regions (orange curve), and complementary regions (blue curve), (A) in the whole BBBO region and (B) cortical BBBO region. The complementary refers to the rest of the hemisphere where BBBO has not been proven. The solid line is the mean over $n = 5$ rats and the shaded regions depict the SE of the mean.

complementary parts ($p=0.05$; paired t -test). Then, the decrease in perfusion subsides to $12.3\% \pm 4.5\%$ ($p = 0.01$; paired t -test) for BBBO regions and $10.0 \pm 7.0\%$ for the complementary regions ($p = 0.04$; paired t -test) at 48 min. On the cortical structure, the measured impact was more pronounced and reached $30.8\% \pm 5.8\%$ decrease at 18 min for BBBO regions ($p = 0.02$; paired t -test) and a $21.4 \pm 7.0\%$ for the complementary ($p = 0.05$; paired t -test).

Then, the decrease in perfusion subsides to $13.0 \pm 7.2\%$ ($p = 0.03$; paired t -test) for BBBO regions and $13.6 \pm 5.3\%$ for the complementary region ($p = 0.17$; paired t -test) at 48 min.

Perfusion maps (Figure 7) obtained by the bolus tracking method are consistent with the last pCASL-CBF measurements obtained before contrast agent injection. Displayed results from DSC-rCBF maps, Figure 8,

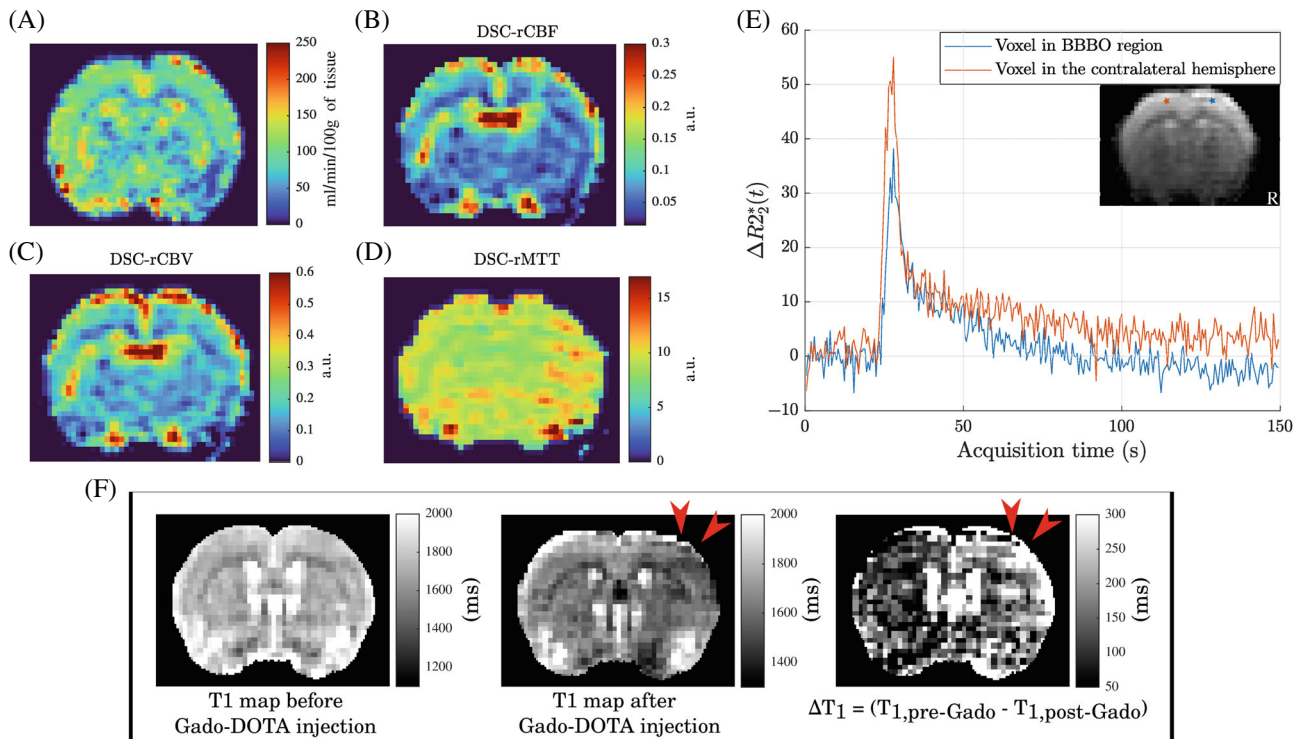


FIGURE 7 Obtained perfusion maps from DSC-MRI for one typical subject compared to (A) pCASL-CBF map; (B) DSC-rCBF map, (C) DSC-rCBV map, and (D) DSC-mean transit time map. (E) BBB opening (BBBO) impact on DSC-MRI time course during the first pass of Gado-Dota bolus (blue curve) compared to DSC-MRI time course in the unexposed hemisphere (orange curve). (F) Corresponding T_1 maps before and after Gadolinium injection and the computed ΔT_1 map from the latter

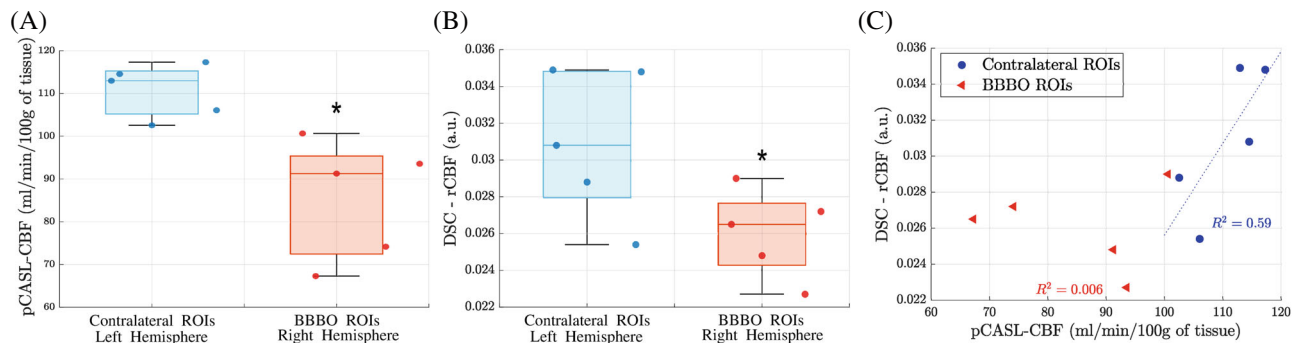


FIGURE 8 Evaluation of cerebral blood flow (CBF) obtained by Arterial Spin Labeling (ASL) and DSC-MRI at 50 min following microbubble intravenous injection (MB+US). (A) pCASL-CBF significantly lower in blood brain barrier opening (BBBO) regions ($p = 0.03$; paired t -test). (B) DSC-rCBF also significantly lower in BBBO regions ($p = 0.004$; paired t -test). (C) pCASL-CBF versus DSC-rCBF scatter-plot for the $n = 5$ animals of the Experiment 2

indicates a $15\% \pm 4\%$ decrease between BBBO region and contralateral region. Meanwhile, pCASL-CBF indicated a $22\% \pm 15\%$ decrease in BBBO regions compared to their contralateral in the non-sonicated hemisphere ($p = 0.04$; paired t -test). The effect of BBB opening on the pCASL-CBF and DSC-rCBF were similar ($p = 0.32$; paired t -test). Nevertheless, the expected correlation between pCASL-CBF and DSC-rCBF, which is observed at the contralateral regions ($R^2 = 0.59$, $p = 0.13$), is

no longer valid in the BBBO regions ($R^2 = 0.006$, $p = 0.9$).

For the estimated cerebral blood volume (rCBV) maps, no significant decrease has been found between BBBO regions (0.31 ± 0.16 a.u.) and contralateral regions (0.35 ± 0.19 a.u.) ($p = 0.06$; paired t -test). A slight increase in the mean transit time was measured in the sonicated area (11.1 ± 2.6 a.u.) compared to its contralateral (10.6 ± 2.3 a.u.) ($p = 0.03$; paired t -test).

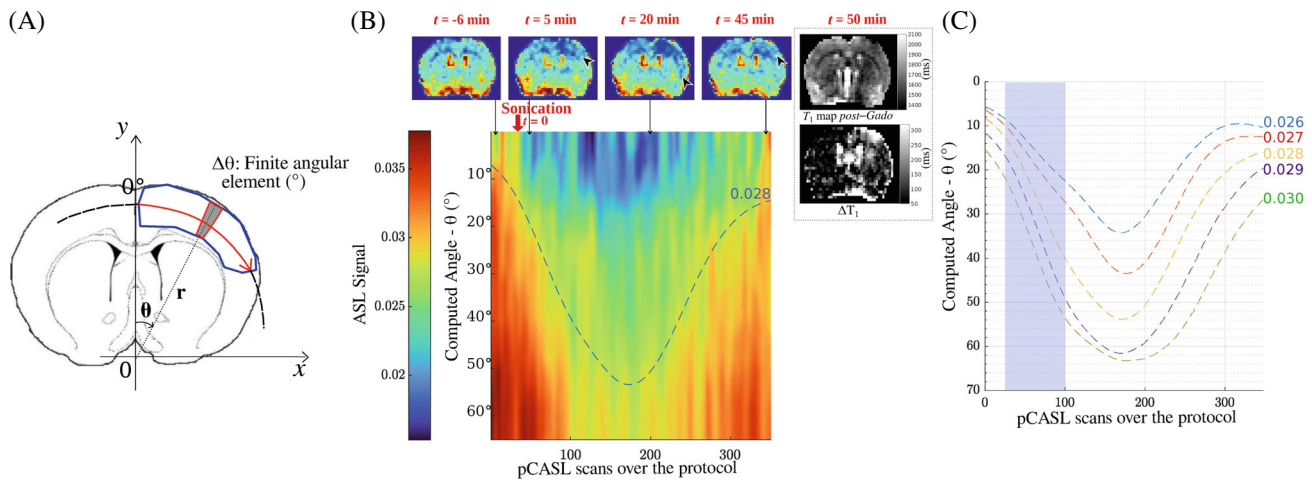


FIGURE 9 Hypoperfusion spreading through the cortex. (A) Representative scheme of the method used to study the propagation of hypoperfusion through the cerebral cortex: for a given center in spherical coordinates (r, θ), cortex voxels were averaged with an angular binning of 0.5° . 0° corresponds to the dorsal part of the cortex, and the angular rotation is clockwise. (B) Obtained map of the cortical spreading hypoperfusion through time. Black arrows on the cerebral blood flow (CBF) maps describe the visible progression of hypoperfusion through the cortex. (C) Level curves plotted for several Arterial Spin Labeling (ASL) signal values as a function of time (pCASL scans). The shaded area indicates the slope considered to calculate the mean propagation velocity of the wave at 0.03 between 7 and 12 min following BBBO procedure.

The ADC maps showed no significant difference between the BBBO regions ($714 \pm 23 \mu\text{m}^2/\text{s}$) and the contralateral regions ($712 \pm 20 \mu\text{m}^2/\text{s}$) ($p = 0.73$; paired t -test).

The spatiotemporal analysis described in Figure 9, allowed us to observe the propagation of the cerebral perfusion decrease from the dorsal cortex to the ventral cortex within a slice. Surprisingly, there is not a strict spatial correspondence between the hypoperfusion spreading and the impact of BBB opening estimated from the difference in T_1 , before and after the contrast agent injection. Indeed, hypoperfusion onset (between 0° and 15°) is more medial than the highest BBBO impact (between 20° and 30°). The mean velocity of the hypoperfusion propagation was estimated to be $560 \pm 45 \mu\text{m}/\text{min}$.

4 | DISCUSSION

The aim of this study was to further investigate the effect of BBB opening using ultrasound combined with microbubble injection on brain perfusion. The results of the experiments highlighted a decrease in CBF with strong evidences of transient nonlocal vasoconstriction, lasting for around 60 min following 0.38 MPa US-induced BBB opening, with a significant impact on ATT. Maximum perfusion decreases and BBBO region volumes were different between the two experimental groups of animals. Difference in attenuation loss due to transmission through the skull could explain that discrepancy. Indeed, effective acoustic pressures estimated from animal weight²² was

0.38 and 0.3 MPa in the first and second group, respectively. In a previous study performed with comparable experimental conditions to our Experiment 1, a similar 50% decrease of CBF was measured.¹⁴

The lack of impact on ADC supports that this BBB opening procedure is safe with no potential cytotoxic edema that could be induced by hypoperfusion³³ neither vasogenic edema by the controlled increase of blood barrier permeability.³⁴

The absolute quantification of cerebral blood flow using ASL is based on biophysical models that describe the longitudinal magnetization evolution of tagged spins, through the successive compartments, from arterial blood to brain tissue.^{35,36} In addition, the role of ATT in precise CBF mapping has been widely discussed.³⁷ Indeed, in the present study, a decrease in CBF combined with an increase in ATT was measured in the BBBO region. Such increase in ATT has been associated with an upstream impact or vasoconstriction at the level of feeding arteries³⁰ or arterioles³⁸ that leads to an underestimation of CBF.^{39,40}

Perfusion mapping, in this article, was achieved using the general kinetic model for CBF quantification²⁶ based on the assumption that labeled water in the blood is a freely diffusible endogenous tracer.^{16,26} However, it has been shown that this assumption is not always valid in the brain,^{41,42} especially for high blood flow rate, where water extraction fraction tends to be lower.⁴³ As a result, the BBB plays a role in the exchange restriction between the vascular environment and the brain tissue. Several studies have

investigated the effect of BBB opening on CBF measurement through intravenous injection of Mannitol^{43,44} and they reported an increase in CBF measured by ASL and DSC-MRI.

Thus, for the same effect, BBB opening by MB+US or by Mannitol injection has contradictory consequences on cerebral blood flow. The above-mentioned elements rule out the hypothesis that the observed hypoperfusion is the consequence of BBB opening and support the assumption that the observed CBF decrease is the result of a myogenic reaction to the mechanical strain applied the vessel walls by oscillating microbubbles during sonication.

Different research groups have studied the secondary effects related to BBB opening using ultrasound combined with microbubble injection.¹⁵ Several evidences suggest that MB+US impacts the cerebral vascular system and affects the proper functioning of cerebral blood flow. An *in vivo* study in mice showed in average a reduction of 60% in the diameter of arteries and arterioles following sonication, as observed by optical imaging, followed by a progressive recovery within 20–600 s.³⁸ Results in rats reported a reduction in vessel diameter in only 25% of the vessels exposed to MB+US.⁴⁵ In the same study, an inverse correlation has been found between vessel size and vasoconstriction impact, with a stronger impact in smaller diameter vessels. Thus, the outcomes described in this article are consistent with previous findings, since the observed CBF reduction can be an effect of vessels vasoconstriction.

BBB plays an essential role in protecting brain tissue but also in mediating and regulating the neurovascular coupling. Evidences from fMRI studies have shown that BBB disruption affects this function through a significant decrease in the neurovascular response to stimulus¹³ without affecting CBF baseline (at rest). However, CBF measurement in this study was performed 1 h following sonication. Given the above-described CBF recovery approximately 1 h after MB+US, the lack of effect on cerebral perfusion is understandable. The same group has demonstrated a reduced functional connectivity, using resting state fMRI, in rats after FUS-BBB opening targeted to the right somatosensory cortex.⁴⁶ However, no clear statement can be made about the changes in CBF through fMRI studies, since the BOLD signal originates from both CBF and CMRO₂ (Cerebral Metabolic Rate of Oxygen) contributions.

Another key element to take into account is the inflammatory response triggered by the BBB disruption. Indeed, some research studies have detected, within the BBB opening area, the presence of inflammatory markers (microglia) by immuno-fluorescent staining.^{47,48} The inflammatory response may interfere with the vascular neuro-regulatory system. However, those studies have not

explored neuroinflammation in the hour following BBB opening and have found inflammatory bio-markers several hours after. Therefore, they could not provide an appropriate answer to the above-mentioned phenomenon, that occurs immediately after MB+US.

The DSC perfusion acquisitions support the hypoperfusion highlighted through pCASL scans. ASL and DSC results are comparable in the non-US exposed hemisphere, in agreement with the literature⁴⁹ whereas this congruence is not valid in the hemisphere with BBB opening. A possible explanation for this is that the increase in surface permeability affects the acquisitions and the respective quantification models related to each method in distinct ways.⁴⁴ Indeed, given the used quantification model,²⁶ assuming that water is a freely diffusible endogenous tracer, pCASL-CBF at high perfusion may be overestimated under BBB disruption,⁴¹ where water in the blood may extravasate more freely. Meanwhile, DSC may overestimate CBF due to the impact of Gado-Dota extravasation on the T_2^* signal change. However, BBB opening is expected to have a larger negative impact on perfusion estimation by DSC than by ASL. In fact, due to the relatively small difference between T_1 relaxation times of blood and tissue compared to water exchange rate across the BBB,⁵⁰ the contributions of intravascular and extravascular labeling to the total ASL signal are difficult to distinguish, despite increased BBB permeability. In addition, a similar weak correlation between CBF values from the ASL and DSC was observed when the transit time is more delayed.⁵¹ This finding supports the observed delayed ATT albeit its estimation has some limitations, notably the limited number of multi-PLD scans in the experiment and a possible variation of CBF during the scans considering the results of Experiment 2.

Expansion of CBF decrease beyond the BBBO region highlights the nonlocal aspect of the observed phenomenon and suggests that hypoperfusion requires lower acoustic pressure than the pressure required to make the BBB permeable to Gado-Dota. In addition, the performed spatiotemporal analysis allows to establish some points of similarity with the cortical spreading depression (CSD) phenomenon. CSD is a relatively slow depolarization wave that leads to the suppression of brain activity. The evolution of CBF over time following electrically induced CSD was investigated,⁵² a transient suppression of brain activity was measured by EEG with a 35% reduction in cerebral blood flow, 4 min following CSD onset and a complete recovery after 200 min following CSD onset. This hypoperfusion spreaded at 5mm/min measured by EEG. Similar results were obtained in mice following CSD induced by traumatic brain injury.⁵³ Nonetheless, the spreading velocity computed with the cortical spreading maps reported in the present study is 10 times slower, and suggests a

dependency between the strength of the induced mechanical stimulation and the spreading velocity of hyperperfusion through the cortex. The effect of CSD on blood flow have been extensively investigated and several studies reported a large transient increase in CBF occasionally preceded by a brief hypoperfusion.⁵⁴ This phenomenon is likely dependent on the used species and the mechanism involved in the induction of CSD.

5 | CONCLUSIONS

This study provided strong evidence of a nonlocal transient hypoperfusion following BBB opening by ultrasound combined with intravenous injection of microbubbles identified using pCASL and DSC-MRI. The reported outcomes are in agreement with previous studies that show a decrease in vascular and neurovascular response in the sonicated region. These results may appear counter-intuitive since we would expect an increase in perfusion correlated with a BBB opening. However, we obviously have to count on the physiological reaction to US stimulation. The analysis of the findings suggests a CSD-like phenomena resulting from the mechanical strain generated by microbubble expansion induced by sonication. Intracranial EEG monitoring following BBB opening can be useful to confirm this hypothesis and better characterize the observed hypoperfusion propagation.

In our study, T_2w , T_1w , and ADC scans showed no abnormal hyper- or hypointense voxels in the target regions, meaning that no MRI-detectable edema nor microhemorrhage was caused by the procedure, confirming that the method can safely and effectively open the BBB, as demonstrated in very recent clinical trials for the treatment of amyotrophic lateral sclerosis, mild Alzheimer's disease or glioblastoma.^{55–57} Investigating the effects of MB+US BBB opening on cerebral perfusion is a crucial element to improve our understanding of this method and to broaden its applications in clinical therapy.

ACKNOWLEDGMENTS

Non-Invasive Exploration service (Dr. C. Pestourie, Dr. J. Piraquive) and animal experiment facilities (C. Baudelin) of the US006/CREFRE-Anexplo Inserm/UT3/ENVT are gratefully acknowledged.

FUNDING INFORMATION

Foundation "Gueules Cassées": grant numbers 70-2019 and 22-2022 to Isabelle Loubinoux; National Research Agency (ANR): Recover (ANR-19-ASTR-0027) to Isabelle Loubinoux.


CONFLICT OF INTEREST

The authors declare no potential conflict of interests.

ORCID

Wafae Labriji  <https://orcid.org/0000-0003-2310-0402>


Julien Clauzel  <https://orcid.org/0000-0002-6683-9154>


Jean-Louis Mestas  <https://orcid.org/0000-0002-4684-6082>

Maxime Lafond  <https://orcid.org/0000-0001-8954-9099>


Cyril Lafon  <https://orcid.org/0000-0003-1550-970X>


Anne-Sophie Salabert  <https://orcid.org/0000-0002-4053-7158>

Lydiane Hirschler  <https://orcid.org/0000-0003-2379-0861>

Jan M. Warnking  <https://orcid.org/0000-0002-1683-5163>

Emmanuel L. Barbier  <https://orcid.org/0000-0002-4952-1240>

Isabelle Loubinoux  <https://orcid.org/0000-0003-4461-0890>

Franck Desmoulin  <https://orcid.org/0000-0003-0560-6266>

REFERENCES

1. Partridge WM. The blood-brain barrier: bottleneck in brain drug development. *NeuroRx*. 2005;2:3-14.
2. Larsen JM, Martin DR, Byrne ME. Recent advances in delivery through the blood-brain barrier. *Curr Top Med Chem*. 2014;14:1148-1160.
3. Gandhi K, Barzegar-Fallah A, Banstola A, Rizwan SB, JNJ R. Ultrasound-mediated blood-brain barrier disruption for drug delivery: a systematic review of protocols, efficacy, and safety outcomes from preclinical and clinical studies. *Pharmaceutics*. 2022;14:833.
4. Pouliopoulos AN, Kwon N, Jensen G, et al. Safety evaluation of a clinical focused ultrasound system for neuronavigation guided blood-brain barrier opening in non-human primates. *Sci Rep*. 2021;11:1-17.
5. Beccaria K, Canney M, Goldwirth L, et al. Opening of the blood-brain barrier with an unfocused ultrasound device in rabbits. *J Neurosurg*. 2013;119:887-898.
6. Tung Y-S, Vlachos F, Choi JJ, Deffieux T, Selert K, Konofagou EE. In vivo transcranial cavitation threshold detection during ultrasound-induced blood-brain barrier opening in mice. *Phys Med Biol*. 2010;55:6141.
7. McDannold N, Vykhodtseva N, Hynynen K. Targeted disruption of the blood-brain barrier with focused ultrasound: association with cavitation activity. *Phys Med Biol*. 2006;51:793.
8. Sheikov N, McDannold N, Vykhodtseva N, Jolesz F, Hynynen K. Cellular mechanisms of the blood-brain barrier opening induced by ultrasound in presence of microbubbles. *Ultrasound Med Biol*. 2004;30:979-989.
9. Sheikov N, McDannold N, Sharma S, Hynynen K. Effect of focused ultrasound applied with an ultrasound contrast agent on the tight junctional integrity of the brain microvascular endothelium. *Ultrasound Med Biol*. 2008;34:1093-1104.

10. Mchedlishvili G. Physiological mechanisms controlling cerebral blood flow. *Stroke*. 1980;11:240-248.
11. Rezaei AR, Ranjan M, D'Haese P-F, et al. Noninvasive hippocampal blood-brain barrier opening in Alzheimer's disease with focused ultrasound. *Proc Natl Acad Sci*. 2020;117:9180-9182.
12. Chu P-C, Liu H-L, Lai H-Y, Lin C-Y, Tsai H-C, Pei Y-C. Neuromodulation accompanying focused ultrasound-induced blood-brain barrier opening. *Sci Rep*. 2015;5:1-12.
13. Todd N, Zhang Y, Livingstone M, Borsook D, McDannold N. The neurovascular response is attenuated by focused ultrasound-mediated disruption of the blood-brain barrier. *Neuroimage*. 2019;201:116010.
14. Stupar V, Delalande A, Collomb N, Rome C, Barbier EL. Impact of focused ultrasound on cerebral blood flow. Paper presented at: Joint Annual Meeting ISMRM-ESMRMB; 2018; Paris, France. Abstract 4928.
15. Todd N, Angolano C, Ferran C, Devor A, Borsook D, McDannold N. Secondary effects on brain physiology caused by focused ultrasound-mediated disruption of the blood-brain barrier. *J Control Release*. 2020;324:450-459.
16. Detre JA, Leigh JS, Williams DS, Koretsky AP. Perfusion imaging. *Magn Reson Med*. 1992;23:37-45.
17. Jahng G-H, Li K-L, Ostergaard L, Calamante F. Perfusion magnetic resonance imaging: a comprehensive update on principles and techniques. *Korean J Radiol*. 2014;15:554-577.
18. Jung Y, Wong EC, Liu TT. Multiphase pseudocontinuous arterial spin labeling (MP-PCASL) for robust quantification of cerebral blood flow. *Magn Reson Med*. 2010;64:799-810.
19. Calamante F, Gadian DG, Connelly A. Quantification of perfusion using bolus tracking magnetic resonance imaging in stroke: assumptions, limitations, and potential implications for clinical use. *Stroke*. 2002;33:1146-1151.
20. Schneider M. Characteristics of sonovue™. *Echocardiography*. 1999;16:743-746.
21. Park J, Zhang Y, Vykhodtseva N, Jolesz FA, McDannold NJ. The kinetics of blood brain barrier permeability and targeted doxorubicin delivery into brain induced by focused ultrasound. *J Control Release*. 2012;162:134-142.
22. O'Reilly MA, Muller A, Hynynen K. Ultrasound insertion loss of rat parietal bone appears to be proportional to animal mass at submegahertz frequencies. *Ultrasound Med Biol*. 2011;37:1930-1937.
23. Hirschler L, Debacker CS, Voiron J, Köhler S, Warnking JM, Barbier EL. Interpulse phase corrections for unbalanced pseudo-continuous arterial spin labeling at high magnetic field. *Magn Reson Med*. 2018;79:1314-1324.
24. Brossard C, Montigon O, Boux F, et al. MP3: medical software for processing Multi-Parametric images pipelines. *Front Neuroinform*. 2020;14:594799.
25. Lee S, Yoo R-E, Choi SH, et al. Contrast-enhanced MRI T1 mapping for quantitative evaluation of putative dynamic glymphatic activity in the human brain in sleep-wake states. *Radiology*. 2021;300:661-668.
26. Buxton RB, Frank LR, Wong EC, Siewert B, Warach S, Edelman RR. A general kinetic model for quantitative perfusion imaging with arterial spin labeling. *Magn Reson Med*. 1998;40:383-396.
27. Dobre MC, Uğurbil K, Marjanska M. Determination of blood longitudinal relaxation time (T1) at high magnetic field strengths. *Magn Reson Imaging*. 2007;25:733-735.
28. Herscovitch P, Raichle ME. What is the correct value for the brain-blood partition coefficient for water? *J Cereb Blood Flow Metab*. 1985;5:65-69.
29. Hirschler L, Munting LP, Khmelinskii A, et al. Transit time mapping in the mouse brain using time-encoded pCASL. *NMR Biomed*. 2018;31:e3855.
30. Thomas DL, Lythgoe MF, Weerd L, Ordidge RJ, Gadian DG. Regional variation of cerebral blood flow and arterial transit time in the normal and hypoperfused rat brain measured using continuous arterial spin labeling MRI. *J Cereb Blood Flow Metab*. 2006;26:274-282.
31. Peruzzo D, Bertoldo A, Zanderigo F, Cobelli C. Automatic selection of arterial input function on dynamic contrast-enhanced MR images. *Comput Methods Programs Biomed*. 2011;104:e148-e157.
32. Boxerman JL, Schmainda KM, Weisskoff RM. Relative cerebral blood volume maps corrected for contrast agent extravasation significantly correlate with glioma tumor grade, whereas uncorrected maps do not. *Am J Neuroradiol*. 2006;27:859-867.
33. Simard JM, Kent TA, Chen M, Tarasov KV, Gerzanich V. Brain oedema in focal ischaemia: molecular pathophysiology and theoretical implications. *Lancet Neurol*. 2007;6:258-268.
34. Su W-S, Tsai M-L, Huang S-L, Liu S-H, Yang F-Y. Controllable permeability of blood-brain barrier and reduced brain injury through low-intensity pulsed ultrasound stimulation. *Oncotarget*. 2015;6:42290.
35. Zhang W, Williams DS, Koretsky AP. Measurement of rat brain perfusion by NMR using spin labeling of arterial water: in vivo determination of the degree of spin labeling. *Magn Reson Med*. 1993;29:416-421.
36. St. Lawrence KS, Wang J. Effects of the apparent transverse relaxation time on cerebral blood flow measurements obtained by arterial spin labeling. *Magn Reson Med*. 2005;53:425-433.
37. Woods JG, Chappell MA, Okell TW. Designing and comparing optimized pseudo-continuous Arterial Spin Labeling protocols for measurement of cerebral blood flow. *Neuroimage*. 2020;223:117246.
38. Raymond SB, Skoch J, Hynynen K, Bacsikai BJ. Multiphoton imaging of ultrasound/Optison mediated cerebrovascular effects in vivo. *J Cereb Blood Flow Metab*. 2007;27:393-403.
39. Fan AP, Guo J, Khalighi MM, et al. Long-delay arterial spin labeling provides more accurate cerebral blood flow measurements in moyamoya patients: a simultaneous positron emission tomography/MRI study. *Stroke*. 2017;48:2441-2449.
40. Dai W, Fong T, Jones RN, et al. Effects of arterial transit delay on cerebral blood flow quantification using arterial spin labeling in an elderly cohort. *J Magn Reson Imaging*. 2017;45:472-481.
41. Parkes LM, Tofts PS. Improved accuracy of human cerebral blood perfusion measurements using arterial spin labeling: accounting for capillary water permeability. *Magn Reson Med*. 2002;48:27-41.
42. St. Lawrence KS, Frank JA, McLaughlin AC. Effect of restricted water exchange on cerebral blood flow values calculated with arterial spin tagging: a theoretical investigation. *Magn Reson Med*. 2000;44:440-449.
43. Silva AC, Zhang W, Williams DS, Koretsky AP, Koretsky AP. Estimation of water extraction fractions in rat brain using magnetic resonance measurement of perfusion with arterial spin labeling. *Magn Reson Med*. 1997;37:58-68.

44. Tanaka Y, Nagaoka T, Nair G, Ohno K, Duong TQ. Arterial spin labeling and dynamic susceptibility contrast CBF MRI in postischemic hyperperfusion, hypercapnia, and after mannitol injection. *J Cereb Blood Flow Metab.* 2011;31:1403-1411.
45. Cho EE, Drazic J, Ganguly M, Stefanovic B, Hynynen K. Two-photon fluorescence microscopy study of cerebrovascular dynamics in ultrasound-induced blood-brain barrier opening. *J Cereb Blood Flow Metab.* 2011;31:1852-1862.
46. Todd N, Zhang Y, Arcaro M, et al. Focused ultrasound induced opening of the blood-brain barrier disrupts inter-hemispheric resting state functional connectivity in the rat brain. *Neuroimage.* 2018;178:414-422.
47. Sinharay S, Tu T-W, Kovacs ZI, et al. In vivo imaging of sterile microglial activation in rat brain after disrupting the blood-brain barrier with pulsed focused ultrasound:[18F] DPA-714 PET study. *J Neuroinflammation.* 2019;16:1-11.
48. Ji R, Karakatsani ME, Burgess M, Smith M, Murillo MF, Konofagou EE. Cavitation-modulated inflammatory response following focused ultrasound blood-brain barrier opening. *J Control Release.* 2021;337:458-471.
49. Khashbat D, Abe T, Ganbold M, et al. Correlation of 3D arterial spin labeling and multi-parametric dynamic susceptibility contrast perfusion MRI in brain tumors. *J Med Invest.* 2016;63:175-181.
50. Dickie BR, Parker GJM, Parkes LM. Measuring water exchange across the blood-brain barrier using MRI. *Prog Nucl Magn Reson Spectrosc.* 2020;116:19-39.
51. Yun TJ, Sohn C-H, Han MH, et al. Effect of delayed transit time on arterial spin labeling: correlation with dynamic susceptibility contrast perfusion magnetic resonance in moyamoya disease. *Invest Radiol.* 2013;48:795-802.
52. Duckrow RB. Regional cerebral blood flow during spreading cortical depression in conscious rats. *J Cereb Blood Flow Metab.* 1991;11:150-154.
53. Bouley J, Chung DY, Ayata C, Brown RH Jr, Henninger N. Cortical spreading depression denotes concussion injury. *J Neurotrauma.* 2019;36:1008-1017.
54. Ayata C, Shin HK, Salomone S, et al. Pronounced hypoperfusion during spreading depression in mouse cortex. *J Cereb Blood Flow Metab.* 2004;24:1172-1182.
55. Abrahao A, Meng Y, Llinas M, et al. First-in-human trial of blood-brain barrier opening in amyotrophic lateral sclerosis using MR-guided focused ultrasound. *Nat Commun.* 2019;10:1-9.
56. Epelbaum S, Burgos N, Canney M, et al. Pilot study of repeated blood-brain barrier disruption in patients with mild Alzheimer's disease with an implantable ultrasound device. *Alzheimers Res Ther.* 2022;14:1-13.
57. Wei H-J, Upadhyayula PS, Pouliopoulos AN, et al. Focused ultrasound-mediated blood-brain barrier opening increases delivery and efficacy of etoposide for glioblastoma treatment. *Int J Radiat Oncol Biol Phys.* 2021;110:539-550.

SUPPORTING INFORMATION

Additional supporting information may be found in the online version of the article at the publisher's website.

Appendix S1. Supporting information

How to cite this article: Labriji W, Clauzel J, Mestas J-L, et al. Evidence of cerebral hypoperfusion consecutive to ultrasound-mediated blood-brain barrier opening in rats. *Magn Reson Med.* 2023;89:2281-2294. doi: 10.1002/mrm.29596